NeuroImage 247 (2022) 118842

Contents lists available at ScienceDirect

NeuroImage

journal homepage: www.elsevier.com/locate/neuroimage

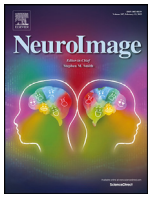

Imaging of cerebral tryptophan metabolism using 7-[^{18}F]FTrp-PET in a unilateral Parkinsonian rat model

Heike Endepols[a,b,c], Boris D. Zlatopolskiy[a,c], Johannes Zischler[a,c], Nazanin Alavinejad[a], Nadine Apetz[a], Stefanie Vus[a,c], Alexander Drzezga[b,e,f], Bernd Neumaier[a,c,d,*]

[a] University of Cologne, Faculty of Medicine and University Hospital Cologne, Institute of Radiochemistry and Experimental Molecular Imaging, Kerpener Str. 62, 50937 Cologne, Germany
[b] University of Cologne, Faculty of Medicine and University Hospital Cologne, Department of Nuclear Medicine, Kerpener Str. 62, 50937 Cologne, Germany
[c] Forschungszentrum Jülich GmbH, Institute of Neuroscience and Medicine, Nuclear Chemistry (INM-5), Wilhelm-Johnen-Straße, 52425 Jülich, Germany
[d] Max Planck Institute for Metabolism Research, Cologne 50931, Germany
[e] German Center for Neurodegenerative Diseases (DZNE), Bonn-Cologne, Germany
[f] Forschungszentrum Jülich GmbH, Institute of Neuroscience and Medicine, Molecular Organization of the Brain (INM-2), Wilhelm-Johnen-Straße, 52425 Jülich, Germany

ARTICLE INFO

Keywords:
Tryptophan
7-[^{18}F]fluorotryptophan
Serotonin
Kynurenine
PET
6-OHDA
Disease models
Animal

ABSTRACT

Degradation products of the essential amino acid tryptophan (Trp) are important signaling molecules in the mammalian brain. Trp is metabolized either through the kynurenine pathway or enters serotonin and melatonin syntheses. The aim of the present work was to examine the potential of the novel PET tracer 7-[^{18}F]fluorotryptophan ([^{18}F]FTrp) to visualize all three pathways in a unilateral 6-OHDA rat model. [^{18}F]FDOPA-PET scans were performed in nine 6-OHDA-injected and six sham-operated rats to assess unilateral dopamine depletion severity four weeks after lesion placement. Afterwards, 7-[^{18}F]FTrp-PET scans were conducted at different timepoints up to seven months after 6-OHDA injection. In addition, two 6-OHDA-injected rats were examined for neuroinflammation using [^{18}F]DAA1106-PET. 7-[^{18}F]FTrp-PET showed significantly increased tracer uptake at the 6-OHDA injection site which was negatively correlated to time after lesion placement. Accumulation of [^{18}F]DAA1106 at the injection site was increased as well, suggesting that 7-[^{18}F]FTrp uptake in this region may reflect kynurenine pathway activity associated with inflammation. Bilaterally in the dorsal hippocampus, 7-[^{18}F]FTrp uptake was significantly decreased and was inversely correlated to dopamine depletion severity, indicating that it reflects reduced serotonin synthesis. Finally, 7-[^{18}F]FTrp uptake in the pineal gland was significantly increased in relation with dopamine depletion severity, providing evidence that melatonin synthesis is increased in the 6-OHDA rat model. We conclude that 7-[^{18}F]FTrp is able to detect alterations in both serotonin/melatonin and kynurenine metabolic pathways, and can be applied to visualize pathologic changes related to neurodegenerative processes.

1. Introduction

Parkinson's disease (PD) is not only associated with progressive degeneration of dopaminergic neurons, but also with pathological alterations of tryptophan (Trp) metabolism (Szabo et al., 2011). Metabolites or degradation products of the essential amino acid Trp are important signaling molecules in the mammalian brain, which vary in concentration according to the individual's physiological condition (Richard et al., 2009). There are three relevant metabolic pathways (Fig. 1): the serotonin and melatonin biosynthesis pathways, and the kynurenine metabolic pathway with the final product nicotinamide adenine dinucleotide (NAD$^+$) (Ruddick et al., 2006; Schwarcz et al., 2012). Several intermediates are biologically active as well, such as kynurenic acid and quinolinic acid in the kynurenine pathway, and N-acetylserotonin (=normelatonin) in the melatonin pathway.

Abbreviations: 6-OHDA, 6-hydroxy-dopamine; DA, dopamine; IDO-1, indoleamine 2,3-dioxygenase 1; KAT, kynurenine aminotransferase; KMO, kynurenine 3-monooxygenase; KYNU, kynureninase; NAD+, nicotinamide adenine dinucleotide; PD, Parkinson's disease; SUVR, standardized uptake value ratio; TFCE, threshold-free cluster enhancement; Trp, tryptophan; VOI, volume of interest.

* Corresponding author at: Forschungszentrum Jülich GmbH, Institute of Neuroscience and Medicine, Nuclear Chemistry (INM-5), Wilhelm-Johnen-Straße, 52425 Jülich, Germany.

E-mail addresses: heike.endepols@uk-koeln.de (H. Endepols), boris.zlatopolskiy@uk-koeln.de (B.D. Zlatopolskiy), nazanin.alavinejad@uk-koeln.de (N. Alavinejad), nadine.apetz@uk-koeln.de (N. Apetz), s.vus@fz-juelich.de (S. Vus), alexander.drzezga@uk-koeln.de (A. Drzezga), b.neumaier@fz-juelich.de (B. Neumaier).

https://doi.org/10.1016/j.neuroimage.2021.118842.
Received 30 July 2021; Received in revised form 30 November 2021; Accepted 19 December 2021
Available online 21 December 2021.

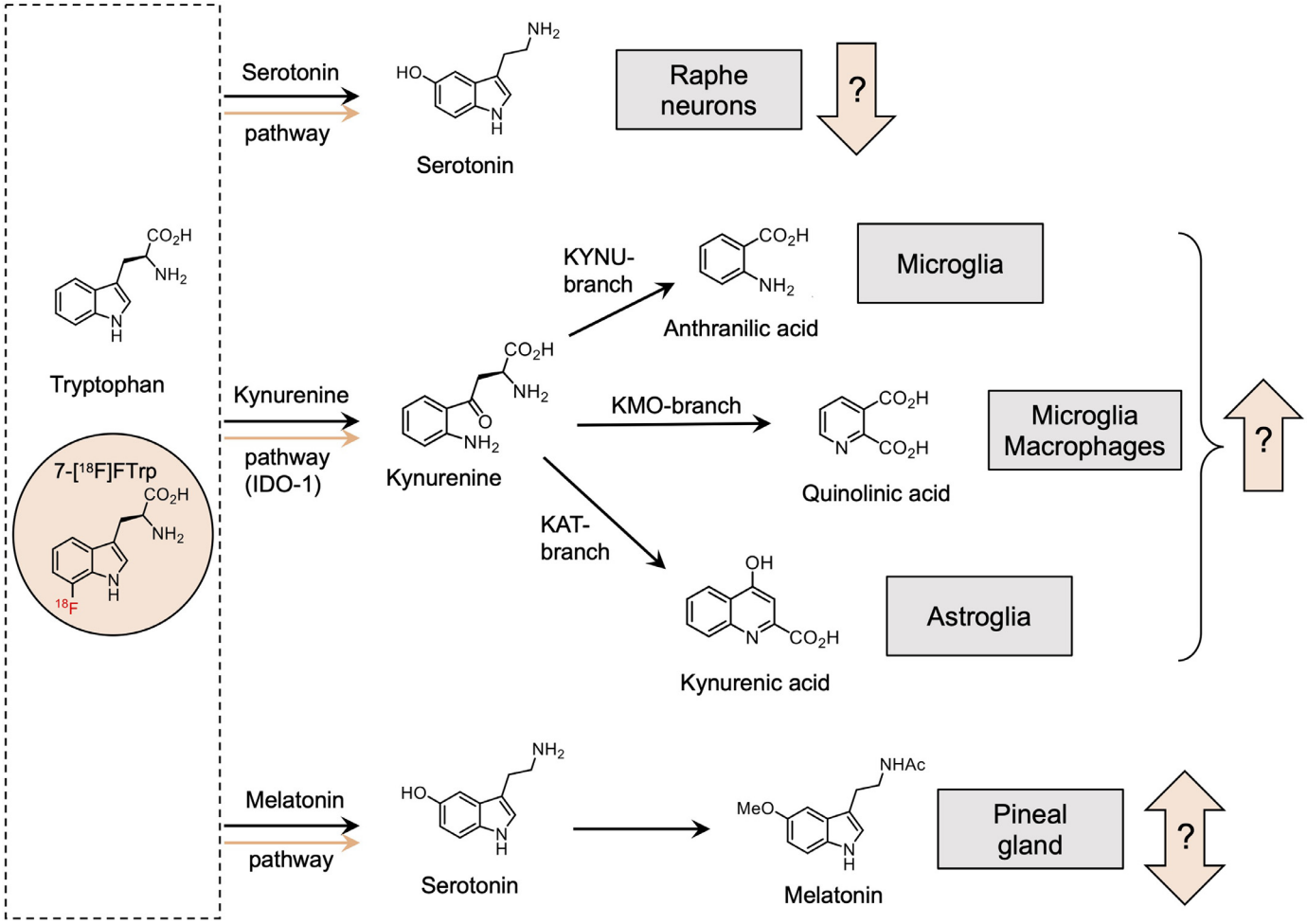

Fig. 1. Metabolic pathways of Trp and their visualization with its PET-analogue 7-[^{18}F]FTrp.

Serotonin is mainly synthesized in neurons of the raphe nuclei, which give rise to a dense network of axonal projections into all regions of the brain (Jacobs and Azmitia, 1992). As a first step, Trp hydroxylase adds a hydroxyl group in position 5 of the indole motif, generating 5-hydroxytryptophan. The second step involves decarboxylation through aromatic amino acid decarboxylase, yielding 5-hydroxytryptamine (=serotonin). Serotonin is produced in cell bodies as well as axon terminals, and can be released from both structures (Best et al., 2010; De-Miguel et al., 2015). Altered (typically decreased) serotonergic activity is well-known to be associated with depression and anxiety (Andrews et al., 2015; Olivier, 2015). In PD, serotonergic neurons progressively degenerate, although with slower progression than dopaminergic neurons (Politis and Niccolini, 2015). Dysfunction of the serotonergic system is associated with tremor, L-DOPA-induced dyskinesias, and non-motor symptoms of PD, such as depression and fatigue (Politis and Loane, 2011; Politis et al., 2014).

Melatonin is produced by N-acetylation and subsequent O-methylation of serotonin in the pineal gland. It is mainly released at night (Tordjman et al., 2017), and reaches the brain through the bloodstream or the pineal recess, which is an evagination of the third ventricle (Tricoire et al., 2002). Melatonin receptors are present in many brain areas, and are involved in sleep, anxiety, pain and circadian rhythm (Ng et al., 2017). There is considerable controversy in the literature about the changes of melatonin production in PD. A recent review summarized that some authors found no change in melatonin homeostasis while others reported phase shifts with decreased production (Mack et al., 2016). Yet another study observed that serum melatonin levels were increased in PD patients and in 6-OHDA rat models, and that there was a significant correlation with disease severity (Lin et al., 2014). A possible explanation for these conflicting findings is that melatonergic changes in PD are highly variable.

The vast majority of Trp that is not consumed by protein synthesis is degraded by the kynurenine pathway (Campbell et al., 2014; Schwarcz et al., 2012). In the brain, the enzyme indoleamine-2,3-dioxygenase 1 (IDO-1) converts Trp to formylkynurenine, which is further transformed into kynurenine by kynurenine formamidase. After that, the kynurenine pathway can proceed through three main branches (Campbell et al., 2014; Schwarcz et al., 2012) that are named after their key enzymes kynurenine aminotransferase (KAT-branch leading to kynurenic acid), kynureninase (KYNU-branch leading to anthranilic acid), and kynurenine 3-monooxygenase (KMO-branch, leading to quinolinic acid and NAD^+). Because of the high affinity of kynurenine for KMO, the KMO branch is the main metabolic pathway in microglia and macrophages, where it gives rise to the excitotoxic NMDA receptor agonist quinolinic acid. The neuroprotective metabolite kynurenic acid on the other hand is mainly produced through the KAT-branch in astrocytes, which can also degrade toxic quinolinic acid formed in other cell types. In PD, there is a general up-regulation of IDO activity (Maddison and Giorgini, 2015), while KAT-branch activity and kynurenic acid production decrease, so that Trp catabolism shifts further towards the KMO branch and increased quinolinic acid production. This abets excitotoxicity caused by quinolinic acid or excess glutamate, which leads to neurotoxicity and cell death (Lim et al., 2017; Tan et al., 2012).

In PD, 7-[^{18}F]FTrp is supposed to display a decrease of serotonin production in raphe neurons, an activation of the kynurenine pathway and alterations (either way) in melatonin production (orange arrows).

Accordingly, PD patients suffer from an imbalance between serotonin production (decrease) and kynurenine pathway activity (increase), with an additional shift towards formation of neurotoxic metabolites in the kynurenine pathway. To therapeutically address these changes, e.g. by applying serotonergic agents (Schrag et al., 2015) or by shifting the kynurenine pathway towards neuroprotective branches (Zadori et al., 2012), a thorough diagnosis of the Trp metabolic state is needed. However, PET imaging of Trp metabolism (Zlatopolskiy et al., 2020) is rarely used for diagnosis in PD patients. Thus, α-[^{11}C]methyl-L-tryptophan as a surrogate marker for both serotonin synthesis and kynurenine pathway metabolism (Chugani and Muzik, 2000; Diksic, 2001) was applied, but the short half-life of carbon-11 limits its use to imaging centers with an on-site cyclotron. In an attempt to circumvent this drawback, our group has recently developed the ^{18}F-labeled Trp analogue 7-[^{18}F]fluorotryptophan (7-[^{18}F]FTrp), which delineates serotonergic brain regions and the pineal gland in healthy rats (Zlatopolskiy et al., 2018). However, it is currently unknown if 7-[^{18}F]FTrp can also be used to visualize kynurenine metabolism. Therefore, the aim of the present work was to examine its potential to facilitate the visualization of all three pathways in a unilateral 6-OHDA rat model. Serotonergic axon terminals are present throughout the brain, so that a certain overlap of serotonin and kynurenine pathways is likely. Previous studies have shown that kynurenine metabolism is indeed altered after intracerebral 6-OHDA injection (Knyihar-Csillik et al., 2006), and that inhibition of IDO-1 has a neuroprotective effect (Sodhi et al., 2021). Furthermore, neuroinflammation is confined to the lesioned hemisphere (Gasparotto et al., 2017; Haas et al., 2016; Koprich et al., 2008), although one study reported widespread (including contralateral) occurrence of activated microglia 28 days after striatal 6-OHDA infusion (Cicchetti et al., 2002). We therefore postulate increased 7-[^{18}F]FTrp uptake ipsilaterally, particularly at the injection site, reflecting increased kynurenine metabolism due to inflammation. To estimate the extent of microglial activation, we performed additional PET scans with the tracer [^{18}F]DAA1106. Decreased 7-[^{18}F]FTrp uptake due to decreased serotonin production is expected to occur in both hemispheres, but will be most obvious contralateral because of the absence of neuroinflammation.

In order to evaluate the relationship between 7-[^{18}F]FTrp uptake and dopamine depletion severity, we conducted PET scans with [^{18}F]FDOPA in the same animals. Our main aim in this study was to visualize chronic alterations of Trp metabolism by means of the PET tracer 7-[^{18}F]FTrp in a unilateral 6-OHDA Parkinsonian rat model and assign them to serotonin, melatonin and kynurenine metabolic pathways.

2. Materials and methods

2.1. Animals

Altogether, 17 adult male Long Evans rats (*Rattus norvegicus*; Janvier, France; three months old at the start of the study) were used. Fifteen rats (328–365 g) were used for the 7-[^{18}F]FTrp study: Nine rats were subjected to unilateral 6-OHDA injections in the medial forebrain bundle, and six rats were sham-operated, as previously described (Apetz et al., 2019; Kordys et al., 2017). All fifteen rats underwent one [^{18}F]FDOPA-PET and one 7-[^{18}F]FTrp-PET scan. To evaluate the influence of neuroinflammation at the 6-OHDA injection site, two additional rats with a 6-OHDA lesion [360 + 387 g] were examined using [^{18}F]DAA1106 and [^{18}F]FDOPA during the first week and four weeks after 6-OHDA injection. To assess the integrity of the serotonergic system in the chronic phase, three rats were sacrificed three, seven and eleven months after 6-OHDA injection for serotonin immunohistochemistry of the dorsal raphe nucleus (see below). Rats were housed in pairs in individually ventilated cages (NextGen, Ecoflow, Phantom, Allentown) under controlled ambient conditions (22 ± 1 °C and 55 ± 5% relative humidity) on an inversed 12 h light/dark schedule (lights on 8:30 pm–8:30 am). They had free access to food and water. Experiments were carried out in accordance with the EU directive 2010/63/EU for animal experiments and the German Animal Welfare Act (TierSchG, 2006) and were approved by regional authorities (LANUV NRW; application number 84-02.04.2012.A304).

2.2. Surgery

Animals were anesthetized (initial dosage: 5% isoflurane in O_2/N_2O (3:7), reduced to 1.5–2.5% isoflurane for maintenance) and received 0.1 ml Carprofen (Rimadyl®, Pfizer, Berlin, Germany) subcutaneously for analgesia. Each animal was fixed on a warming pad in a stereotactic system with a motorized stereotactic drill and injection robot (Robot Stereotaxic, Neurostar®, Tübingen, Germany). For lesion generation, 21 µg 6-hydroxy-dopamine (6-OHDA) hydrobromide stabilized with ascorbic acid (Sigma Aldrich; equals 14 µg of 6-OHDA free base) in 3 µL NaCl was injected unilaterally into the medial forebrain bundle (n = 9; coordinates: - 4.4 mm posterior, 1.2 mm lateral, 7.9 mm ventral to Bregma). In sham animals (n = 6), 3 µL NaCl were injected into the same region. Injection side (left/right) was randomized.

2.3. MRI measurements

One day after 6-OHDA/sham injection, all rats underwent a structural MRI scan under 2% isoflurane anesthesia. T_2-weighted, rapid acquisition with relaxation enhancement (RARE) images were recorded with an 11.7-T BioSpec animal scanner (Bruker BioSpin®, Billerica, MA, USA) by using a quadrature receive-only rat brain surface coil (Bruker BioSpin®) in combination with an actively decoupled, transmit-only quadrature resonator (Bruker BioSpin®), fitting into the BFG-150/90-S14 combined gradient and shim set (Resonance Research Inc., Billerica, MA, USA).

2.4. PET measurements

Fifteen rats (9 6-OHDA, 6 shams) were measured with both 6-[^{18}F]fluoro-L-3,4-dihydroxyphenylalanine ([^{18}F]FDOPA)- (Zarrad et al., 2017) and 7-[^{18}F]FTrp-PET (Zlatopolskiy et al., 2018) in list mode using a Focus 220 micro PET scanner (CTI-Siemens, Germany) with a resolution at center of field of view of 1.4 mm. [^{18}F]FDOPA-PET scans took place four weeks after the 6-OHDA/sham lesion. First, 15 mg/kg benserazide (Sigma-Aldrich; Steinheim, Germany) was injected intraperitoneally to block peripheral decarboxylation of [^{18}F]FDOPA. 50 min after benserazide injection, rats were anesthetized (initial dosage: 5% isoflurane in O_2/air (3:7), then reduction to 2%), and a catheter for tracer injection was inserted into the lateral tail vein. Rats were placed on an animal holder (Medres, Cologne, Germany), and fixed with a tooth bar in a respiratory mask. Breathing rate was monitored and kept at around 60 breaths per min by adjusting the isoflurane concentration (1.5–2.5%). Body temperature was maintained at 37 °C by a feedback-controlled system. 54–71 MBq of [^{18}F]FDOPA in 500 µl NaCl were injected into the lateral tail vein at the start of the 60 min emission scan, followed by a 10 min transmission scan with a rotating ^{57}Co point source for attenuation correction.

7-[^{18}F]FTrp-PET measurements were conducted over a period of one to seven months after placement of the 6-OHDA/sham lesion. For timepoints see Inline Supplementary Fig. S1. The procedure was carried out as described above, except that the animals were not pre-treated with benserazide. 45–71 MBq of 7-[^{18}F]FTrp in 500 µL NaCl were injected i.v. at the start of the 120 min emission scan, which was followed by a ^{57}Co transmission scan (10 min) for attenuation correction. All 7-[^{18}F]FTrp-PET scans were performed in the rats' dark phase (lights off at 8:30 a.m. in the animal room) with tracer injection between 11:48 a.m. and 3:39 p.m. During the scan, the overhead lights were switched on, and natural daylight came from the window near the scanner. The rats' eyes were

open and protected from drying with eye and nose cream (Bepanthen, Bayer Vital GmbH).

Two additional 6-OHDA-lesioned rats underwent PET scans with [^{18}F]DAA1106 (Zlatopolskiy et al., 2015), which binds to the translator protein 18 kDa and visualizes activated microglia (Schroeder et al., 2021). They were measured 4 days and 32 days after 6-OHDA injection (71–78 MBq i.v.). The same animals underwent [^{18}F]FDOPA-PET at 7 days and 30 days after 6-OHDA-injection (50–78 MBq). The emission scan started with tracer injection ([^{18}F]DAA1106) or 30 min after tracer injection ([^{18}F]FDOPA), lasted 30 min, and was followed by a ^{57}Co transmission scan (10 min).

2.5. Image reconstruction and analysis

After Fourier rebinning, images were reconstructed into 30 min-frames using the iterative OSEM3D/MAP procedure (Qi et al., 1998) resulting in voxel sizes of 0.38 × 0.38 × 0.80 mm. For [^{18}F]FDOPA image analysis, the second frame (30–60 min p.i.) was used, while the fourth frame (90–120 min p.i.) was used for 7-[^{18}F]FTrp image analysis. For post-processing and image analyses the software VINCI 4.72 (Max Planck Institute for Metabolism Research, Cologne, Germany) was used. Images were co-registered manually to the Swanson rat brain atlas (Swanson, 2003), smoothed with a Gauss kernel of 1.5 mm FWHM and intensity normalized to the cerebellum (SUVR = individual voxel value divided by mean value of cerebellum; [^{18}F]FDOPA and 7-[^{18}F]FTrp) or brain background ([^{18}F]DAA1106). Images with right hemispheric injections were flipped so that the intervention was always displayed on the left. The [^{18}F]FDOPA images were used to calculate dopamine depletion severity: Basal ganglia (BG) volumes of interest (VOIs), which covered striatum and nucleus accumbens, were drawn ipsi- and contralesional, and VOI mean values were extracted. A dopamine depletion severity score (dimensionless) was calculated as 1-($SUVR_{BG}$ ipsilesional/$SUVR_{BG}$ contralesional).

7-[^{18}F]FTrp uptake differences between 6-OHDA and sham group were calculated using a voxel-wise *t*-test. This was followed by a threshold-free cluster enhancement (TFCE) procedure (Smith and Nichols, 2009), which includes correction for multiple testing on the $p < 0.05$ significance level. In addition to the voxel-wise comparisons, several VOIs were generated: Injection site (covering the area of edema and inflammation, see insert of Fig. 2), pineal gland, and dorsal hippocampus. For the dorsal hippocampus, four VOIs were established: Two VOIs overlapping with the ipsi- and contralesional significant clusters (Fig. 2 E3), and two anatomical VOIs derived from the MRI template. Two Pearson correlation analyses were performed to assess the relationship between mean VOI 7-[^{18}F]FTrp uptake and either dopamine depletion severity or time after 6-OHDA lesion. All animals were pooled for correlation analysis.

2.6. Immunohistochemistry

Rats were transcardially perfused with 4% paraformaldehyde solution in phosphate buffered saline (PBS), brains were extracted and post-fixed for at least 48 h. Subsequently, brains were transferred to a 30% sucrose solution. After the brains sunk to the bottom of the vessel, which took at least 72 h, they were frozen in a Leica CM1950 cryostat and cut into transverse sections of 30 µm. For antigen demasking, sections were immersed in 0.01 M sodium citrate buffer (pH 6.0) and heated to 97 °C for 10–15 min in a microwave. Sections were then incubated in 3% H_2O_2 in methanol for 3–5 min to quench endogenous peroxidase activity. Subsequently, sections were incubated with blocking serum (10% normal goat serum; Vector) for 1 h. The primary antibody (polyclonal rabbit anti-5-HT, Immunostar) was applied at a dilution of 1:500 at 4 °C overnight. Afterwards, the secondary antibody (anti-rabbit IgG) from the rabbit Vectastain ABC kit was applied according to the manufacturer's instructions for 1 h at room temperature. The sections were then incubated with the avidin-biotin complex from the rabbit Vectastain ABC kit for 30 min. Finally, sections were incubated in diaminobenzidine solution (SigmaFast tablets, 0.35 mg/mL 3,3′-diaminobenzidine, Sigma-Aldrich + 0.3 µL/mL 30% H_2O_2) for 10 min, dehydrated in an ascending alcohol series, immersed in Roti-Histol for 2 min, and then coverslipped in Entellan.

3. Results

[^{18}F]FDOPA-PET showed a strong reduction of tracer uptake in the ipsilesional basal ganglia (= striatum and nucleus accumbens) four weeks after 6-OHDA injection (Fig. 2 A1, A2, white arrows; see Inline Supplementary Figs. S2 + S3). The dopamine depletion severity score (dimensionless) amounted to 0.18 ± 0.02 in 6-OHDA-injected rats ($n = 9$), and 0.01 ± 0.02 in sham rats, which means that ipsilesional [^{18}F]FDOPA uptake was approx. 18% lower than contralesional uptake, with a noise level of approx. 1%. At the 6-OHDA injection site, [^{18}F]FDOPA uptake was increased after one week (Fig. 4C+E), but returned to baseline levels (SUVR 1.02 ± 0.05) after four weeks and was the same as in sham animals (SUVR 1.03 ± 0.12; Figs. 2 A4, B4).

7-[^{18}F]FTrp-PET revealed a higher mean tracer uptake at the 6-OHDA injection site compared to the NaCl injection site in sham animals (Fig. 2 C4, blue arrow). The voxel-wise *t*-test demonstrated that the increase of 7-[^{18}F]FTrp uptake in 6-OHDA animals was statistically significant in a small cluster (4 voxels) at the center of the injection site (Fig. 2 E4, red voxels). When VOI values of the whole injection site were compared, no significant difference was found between 6-OHDA rats (SUVR 1.14 ± 0.09) and shams (SUVR 1.12 ± 0.06; $p = 0.5744$). However, a strong negative correlation was found between 7-[^{18}F]FTrp uptake in the injection site VOI and time after lesion placement (Table 1; Fig. 3A2; 6-OHDA and shams were pooled for correlation analysis). This indicates that tracer uptake was initially increased at the injection site but this effect faded with time.

Mean 7-[^{18}F]FTrp uptake in the dorsal hippocampus of 6-OHDA rats showed a bilateral reduction when compared to shams (Fig. 2 C3, yellow arrows). Voxel-wise comparison revealed statistically significant differences for two clusters in the ipsi- and contralesional dorsal hippocampus (Fig. 2 E3+E4, blue voxels). Comparison of the anatomical hippocampal VOIs yielded a statistic tendency ($p = 0.0712$) for the contralesional but not ipsilesional ($p = 0.3225$) dorsal hippocampus. For both dorsal hippocampal clusters, a negative correlation was found with dopamine depletion severity (Table 1, Fig. 3B1). This indicates that the higher unilateral striatal dopamine depletion, the lower was the dorsal hippocampal 7-[^{18}F]FTrp uptake both ipsi- and contralesional. Dorsal hippocampal 7-[^{18}F]FTrp uptake showed no correlation with time after the lesion, indicating that reduced uptake was a robust phenomenon occurring throughout the investigated chronic phase between one and seven months after lesion placement.

A higher 7-[^{18}F]FTrp uptake was found in the pineal gland of 6-OHDA rats compared to shams (Fig. 2 C5, orange arrow). VOI analysis revealed a statistic tendency (6-OHDA SUVR 1.21 ± 0.14; sham SUVR 1.08 ± 0.1; $p = 0.0645$; Tab 1). 7-[^{18}F]FTrp uptake in the pineal gland was neither correlated with the time of day ($R = 0.27$, $p = 0.3929$; tracer injection between 11:48 a.m. and 3:39 p.m. during the rats' dark phase, which began at 8:30 a.m.), nor with the elapsed time after lesion (Table 1). This confirms that altered 7-[^{18}F]FTrp uptake cannot be explained by a natural fluctuation which may occur during the four hours of our measurement time window, and also not by short-term lesion effects or aging.

The [^{18}F]DAA1106 images, taken four days and four weeks after 6-OHDA injection, revealed strong microglial activation around the injection site at both timepoints (Fig. 4B+D). Accordingly, neuroinflammation at the injection site persists for at least four weeks.

Serotonin immunohistochemistry of the dorsal raphe nucleus showed that 6-OHDA injection was not associated with an obvious loss of serotonergic neurons (Fig. 5).

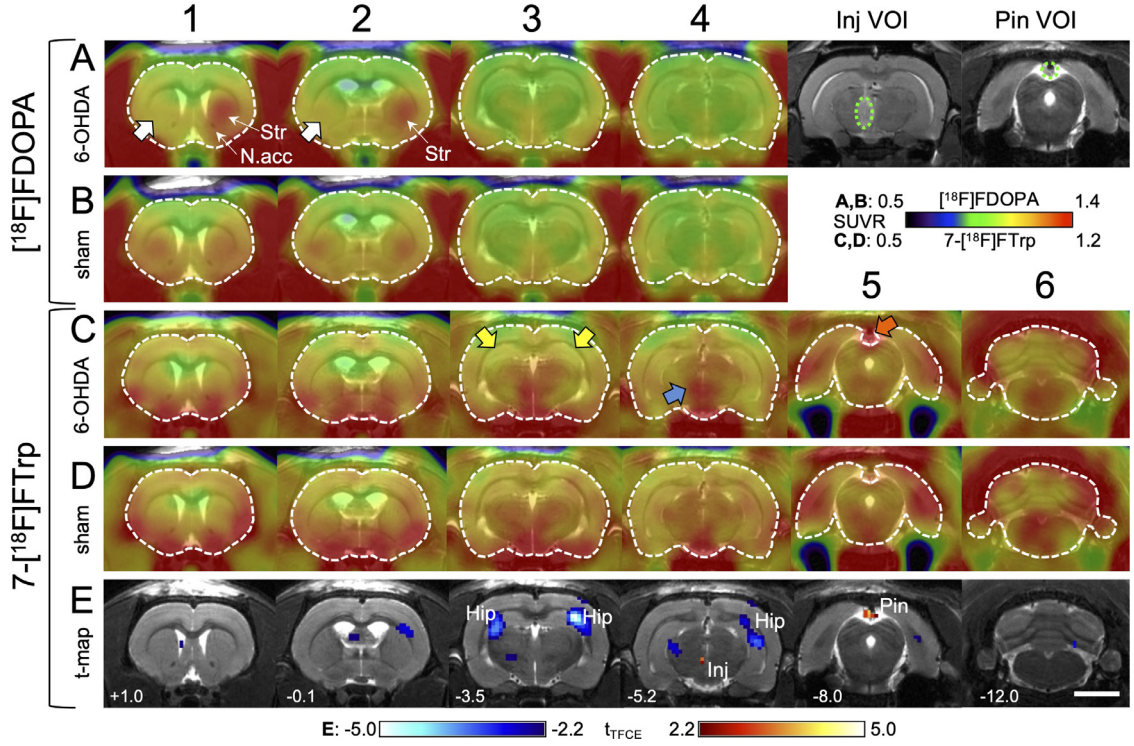

Fig. 2. Changes of Trp metabolism in relation to dopamine depletion severity.
Columns 1–6 indicate transverse section levels. Rostrocaudal coordinates in mm relative to Bregma are shown in row E. **(A)**: Mean [^{18}F]FDOPA images (obtained after four weeks) from $n = 9$ rats infused with 6-OHDA into the medial forebrain bundle, projected onto an MRI template. Images with right-hemispheric lesions were flipped so that dopamine depletion (white arrow) is always shown on the left. The structural T_2-weighted MR images of one single animal taken after 24 h show the volumes of interest covering the injection site (Inj VOI) and the pineal gland (Pin VOI). **(B)**: Mean [^{18}F]FDOPA images from $n = 6$ sham rats. **(C)**: Mean 7-[^{18}F]FTrp images of the same rats as shown in A (taken between 30 and 207 days after 6-OHDA infusion). Increased 7-[^{18}F]FTrp uptake compared to shams is visible at the injection site (blue arrow) and in the pineal gland (orange arrow). Decreased 7-[^{18}F]FTrp uptake is evident bilaterally in the dorsal hippocampus (yellow arrows). **(D)**: Mean 7-[^{18}F]FTrp images of the same sham rats as shown in B. **(E)**: Difference of 7-[^{18}F]FTrp uptake in 6-OHDA versus sham rats. Blue voxels: sham > 6-OHDA. Red voxels: 6-OHDA > sham. $p < 0.05$, corrected for multiple testing. Abbreviations: Hip: hippocampus; Inj: injection site; N.acc: nucleus accumbens; Pin: pineal gland; Str: striatum. Scale bar: 5 mm (For interpretation of the references to color in this figure legend, the reader is referred to the web version of this article.).

Table 1.
7-[^{18}F]FTrp uptake group comparison and correlation (ρ) with dopamine depletion severity (dop) and time-point of measurement (time; range 1–7 months after lesion).

	SUVR sham	SUVR 6-OHDA	SUVR ρ dop	SUVR ρ time
whole injection site	1.12 ± 0.06	1.14 ± 0.09$p = 0.5744$	R= -0.01, $p = 0.9609$	R= -0.80*, $p = 0.0004$
right cluster hippocampus	1.07 ± 0.05	0.95 ± 0.04*$p = 0.0001$	R= -0.69*, $p = 0.0047$	R= -0.08, $p = 0.7671$
left cluster hippocampus	1.02 ± 0.05	0.91 ± 0.04*$p = 0.0006$	R= -0.61*, $p = 0.0162$	$R = 0.18$, $p = 0.5141$
pineal gland	1.08 ± 0.10	1.21 ± 0.14$p = 0.0645$	$R = 0.59$*, $p = 0.0213$	R= -0.03, $p = 0.9074$

4. Discussion

In this study we assessed focal cerebral 7-[^{18}F]FTrp distribution in a unilateral 6-OHDA Parkinsonian rat model in comparison to sham-injected controls. [^{18}F]FDOPA PET was employed to estimate unilateral dopamine depletion severity in the same animals. While [^{18}F]FDOPA measurements were performed exactly four weeks after 6-OHDA injection, 7-[^{18}F]FTrp PET measurements were spread between one and seven months after 6-OHDA injection. This was done to facilitate correlation analysis between 7-[^{18}F]FTrp uptake and time after 6-OHDA/sham injection. The correlation coefficient is an important marker to distinguish between reversible changes in 7-[^{18}F]FTrp uptake directly caused by substance injection (e.g. neuroinflammation, which should abate with time) and persistent alterations caused by death of serotonergic neurons or permanent synaptic changes.

We identified two brain regions where 7-[^{18}F]FTrp uptake was different in the unilaterally 6-OHDA-injected rats compared to sham-injected controls: (1) The injection site where 7-[^{18}F]FTrp uptake was increased in Hemiparkinsonian rats and negatively correlated with time after injection. (2) Two clusters in the dorsal hippocampus where 7-[^{18}F]FTrp uptake was bilaterally decreased in Hemiparkinsonian rats, reduction was stable over time, and negatively correlated with dopamine depletion severity. [^{18}F]DAA1106 PET four weeks after 6-OHDA injection revealed strong microglial activation at the injection site. Thus, increased 7-[^{18}F]FTrp uptake at the injection site could reflect increased kynurenine metabolic pathway activity, which is closely associated with neuroinflammation (Badawy, 2017). We have shown previously that microglial activation can persist for up to six months (Schroeder et al., 2021). A non-selective increase of 7-[^{18}F]FTrp uptake via the LAT1 amino acid transport system may have played a role during the acute phase, but can be ruled out in the chronic phase. The latter can be inferred from [^{18}F]FDOPA uptake, which is mediated by the LAT1 system as well (Kageyama et al., 2000) and showed no increase at the injection site after four weeks. Although 7-[^{18}F]FTrp accumulation at the injection site decreased with time, the highest uptake in 6-OHDA injected rats was measured after 104 days (see Fig. 3A2). This demon-

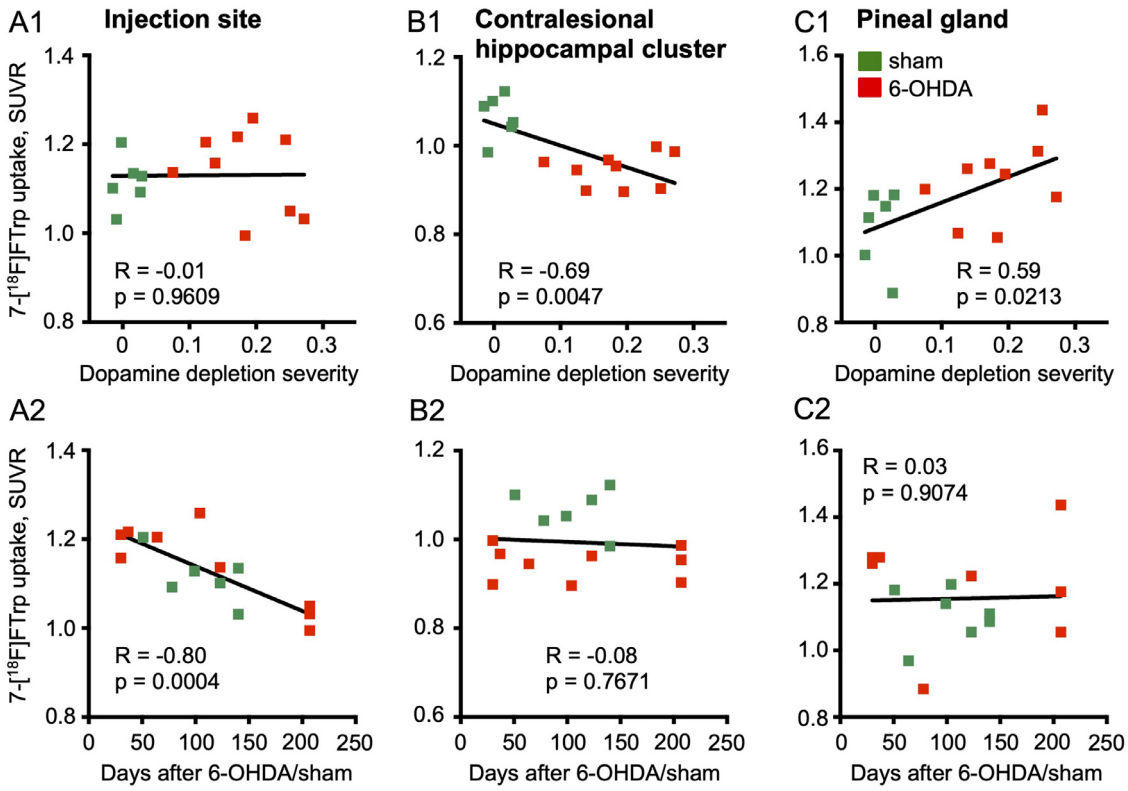

Fig. 3. Pearson correlation of 7-[^{18}F]FTrp uptake with dopamine depletion severity (row 1) and elapsed time after 6-OHDA/sham injection (row 2). **(A):** Injection site. **(B):** Contralesional hippocampus cluster. **(C):** Pineal gland. Regression lines are plotted for better visibility. The dopamine depletion severity score is a dimensionless value, calculated as 1-($SUVR_{BG}$ ipsilesional / $SUVR_{BG}$ contralesional).

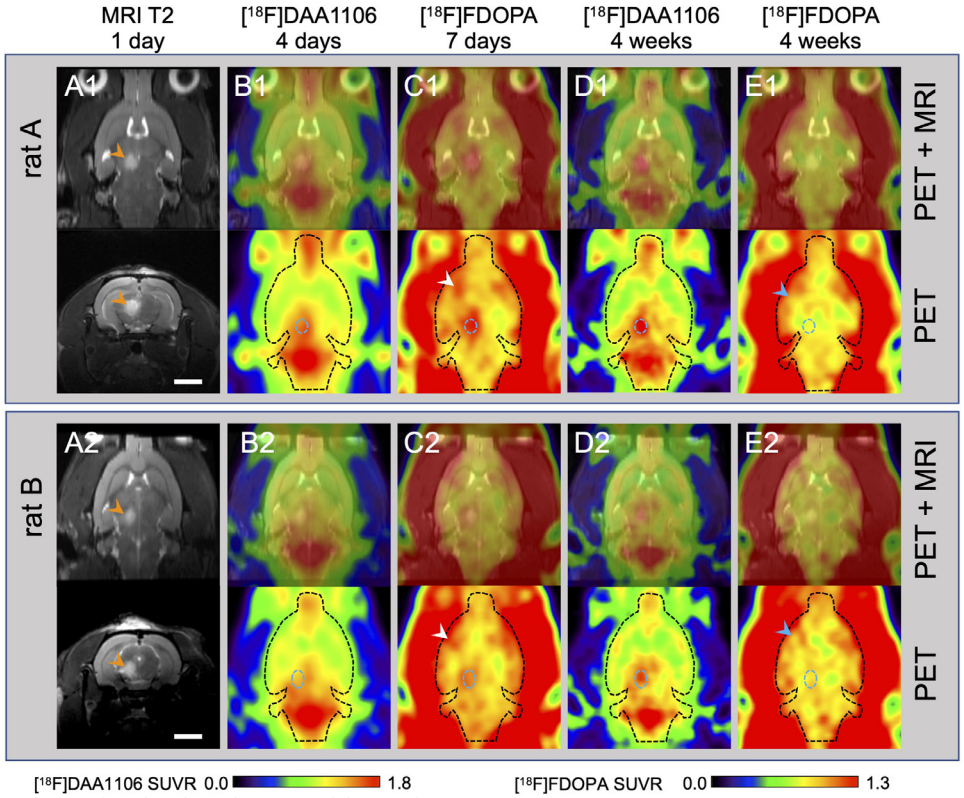

Fig. 4. Relationship between [^{18}F]DAA1106 (neuroinflammation) and [^{18}F]FDOPA uptake (dopamine synthesis) in a unilateral 6-OHDA Parkinsonian rat model. Shown are horizontal sections through the brains of two animals, which received MRI and four PET measurements each. The PET images are projected onto the individual MR images (upper rows) as well as displayed alone (lower rows). The outlines of the brain (black dashed line) and the injection site (blue dashed line) are indicated. **A**: T_2-weighted MRI 24 h after 6-OHDA injection in horizontal and transverse view. The edema caused by the neurotoxin is clearly visible (orange arrowheads) and delineates the injection site. **B**: Uptake of the TSPO-ligand [^{18}F]DAA1106 four days after 6-OHDA injection. Note that increased [^{18}F]DAA1106 uptake is observed around the injection site. **C**: [^{18}F]FDOPA-PET one week after 6-OHDA injection. [^{18}F]FDOPA uptake is increased at the injection site and in the ipsilesional striatum (white arrowheads). **D**: [^{18}F]DAA1106-PET four weeks after 6-OHDA injection. TSPO expression is still widespread, but highly concentrated at the injection site. **E**: [^{18}F]FDOPA-PET four weeks after 6-OHDA injection. There is only baseline uptake at the injection site and reduced uptake in the striatum (blue arrowheads). Scale bar: 5 mm (For interpretation of the references to color in this figure legend, the reader is referred to the web version of this article.).

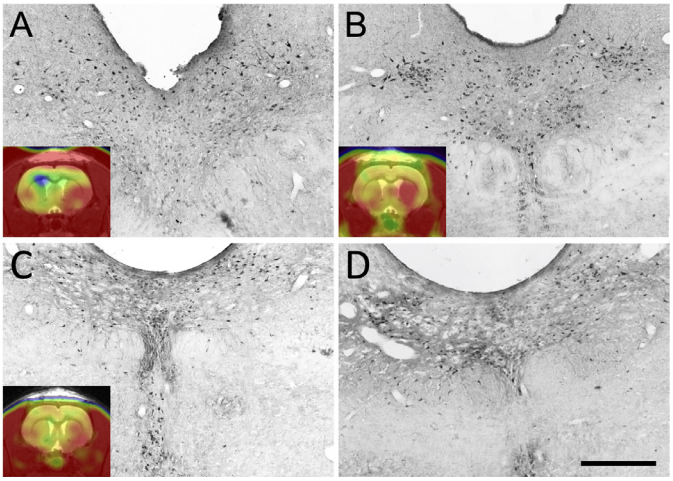

Fig. 5. Serotonin immunohistochemistry in the dorsal raphe nucleus of three different Hemiparkinsonian rats. Lesion is always on the left side. Time-point after 6-OHDA lesion **(A):** Three months. **(B)**: Seven months. **(C+D):** Eleven months, two different section levels. The inserts show the corresponding [^{18}F]FDOPA-PET images at the level of the striatum. Scale bar: 500 μm.

strates that a neurotoxin such as 6-OHDA can cause long-term changes of Trp metabolism, most likely via the kynurenine metabolic pathway (Knyihar-Csillik et al., 2006).

The bilateral decrease of 7-[^{18}F]FTrp accumulation in the hippocampus on the other hand cannot be attributed to the kynurenine metabolic pathway, because IDO-1 expression is already very low in the healthy brain (Dang et al., 2000) and unlikely to decrease any further. This and the fact that 7-[^{18}F]FTrp accumulation was negatively correlated with dopamine depletion severity suggests that the decreased uptake of 7-[^{18}F]FTrp reflects impairment of the serotonin pathway. This would be in line with a previous study, which found a bilateral reduction of *trans*-[^{18}F]Mefway (a serotonin 1A receptor ligand) binding in the hippocampus of rats with unilateral 6-OHDA lesions (Lee et al., 2014). The dorsal hippocampus receives strong serotonergic input from the median raphe nucleus (Azmitia, 1981; Köhler and Steinbusch, 1982; Vertes et al., 1999). Serotonergic neurons from the lateral parts of the nucleus either project to the ipsilateral or to the contralateral hippocampus (with equal strengths), while bilaterally projecting neurons are located on the median raphe midline (Azmitia, 1981). This fact explains the bilateral effect of unilateral 6-OHDA injection on hippocampal 7-[^{18}F]FTrp uptake. However, it is unclear if raphe neurons merely have decreased their serotonin synthesis, or if a considerable number of serotonergic neurons have died after 6-OHDA infusion. Although a systematic immunohistological analysis was beyond the scope of this study, we performed immunohistochemistry with four unilaterally 6-OHDA lesioned animals. Our immunohistological stainings revealed no obvious difference in the numbers of ipsi- and contralesional serotonergic neurons in the rostral raphe group. This is in line with previous reports, indicating that while bilateral 6-OHDA injections have a more severe effect on serotonergic neurons (Eskow Jaunarajs et al., 2012), unilateral injections do not decrease the number of serotonergic dorsal raphe neurons (Berghauzen-Maciejewska et al., 2016). Because we did not find a reduction of 7-[^{18}F]FTrp in other forebrain areas rich in serotonergic projections (e.g. hypothalamus or amygdala), a significant global degeneration of serotonergic neurons or even an overall reduction of serotonin synthesis in our 6-OHDA model is unlikely. We therefore postulate that the decrease of serotonin production is selective for the median raphe-dorsal hippocampus projection. A possible explanation could be that 6-OHDA causes a selective down-regulation of serotonin transporters in the hippocampus (Berghauzen-Maciejewska et al., 2016). This could in turn result in a strong occupation of 5-HT1 autoreceptors (Berumen et al., 2012), with an associated inhibition of serotonin release and synthesis. A recent study reported that after unilateral 6-OHDA infusion in the striatum, binding of the 5-HT1A tracer [^{18}F]Mefway in the hippocampus positively correlated with striatal dopamine transporter availability (Lee et al., 2015). This could point to increasing hippocampal 5-HT1 receptor occupancy by endogenous serotonin with increasing dopaminergic lesion severity. Evidence for decreased serotonin tissue concentrations was found in the hippocampus after unilateral 6-OHDA infusion in the substantia nigra pars compacta (Pierucci et al., 2009). The effect was bilateral, but stronger on the contralateral side, which is in excellent agreement with our findings. However, another study found a reduction of tissue serotonin levels in the ipsi- but not contralesional hippocampus (Kaminska et al., 2017), while a third publication reported that no change was detectable (Liu et al., 2019). This indicates that the degree of disturbance in the hippocampal serotonergic system may be variable in the unilateral 6-OHDA rat model. Further studies are needed to address this point.

In addition to the changes at the 6-OHDA injection site and in the hippocampus, we found significantly increased 7-[^{18}F]FTrp uptake in the pineal gland of 6-OHDA-infused rats, which was positively correlated with dopamine depletion severity. It is conceivable that the increased pineal 7-[^{18}F]FTrp uptake reflects elevated synthesis of melatonin, either through increased Trp uptake via the amino acid uptake system T (Gutierrez et al., 2003) or increased Trp hydroxylase activity (Barbosa et al., 2008). Earlier studies have shown that striatal as well as serum melatonin levels are increased in 6-OHDA rat models, which is particularly evident in the chronic stage six weeks after lesion placement (Lin et al., 2014, 2013). It is unclear if this can be considered a compensatory up-regulation, since there is considerable debate about whether melatonin acts as a neuroprotective or neurodegenerative agent in PD patients and animal 6-OHDA models (Mack et al., 2016).

5. Conclusions

Using the tracer 7-[^{18}F]FTrp, we demonstrated chronic changes of Trp metabolism at the injection site, bilaterally in the hippocampus and in the pineal gland of 6-OHDA-infused rats. These effects were detectable for more than 200 days after lesion placement. This demonstrates that pathological alterations of serotonin and melatonin production as well as kynurenine pathway activity can be persistent, even when dopaminergic neurodegeneration is not further progressing. With 7-[^{18}F]FTrp, we were able to detect these alterations in brain regions with tentative association to either the serotonin, melatonin or kynurenine pathways of Trp metabolism. Trp analoga such as 7-[^{18}F]FTrp may be suitable to image the integrity of serotonin/melatonin systems in PD patients as well. Because in patients, changes in serotonin and kynurenine metabolism may take place in the same brain areas, our next step will be to develop PET tracers which selectively address either serotonin/melatonin production or kynurenine metabolism respectively.

Data and code availability

The PET data sets are stored in a repository:
https://doi.org/10.26165/JUELICH-DATA/MGRYJV
The PET analysis software VINCI (Max Planck Institute for Metabolism Research) is freely available (for academia) at:
http://vinci.sf.mpg.de
There are software versions for MS Windows, Linux and MacOS.

Data availability

The PET datasets are available at: https://doi.org/10.26165/JUELICH-DATA/MGRYJV

Ethics statement

Experiments were carried out in accordance with the EU directive 2010/63/EU for animal experiments and the German Animal Welfare Act (TierSchG, 2006) and were approved by regional authorities (LANUV NRW; application number 84–02.04.2012.A304).

Declaration of Competing Interest

The authors have no conflicts of interest or competing interests to declare that are relevant to the content of this article.

Credit authorship contribution statement

Heike Endepols: Conceptualization, Investigation, Formal analysis, Writing – original draft, Funding acquisition, Writing – review & editing. **Boris D. Zlatopolskiy:** Conceptualization, Resources, Writing – review & editing, Funding acquisition. **Johannes Zischler:** Resources, Writing – review & editing. **Nazanin Alavinejad:** Investigation, Writing – review & editing. **Nadine Apetz:** Investigation, Resources, Writing – review & editing. **Stefanie Vus:** Investigation, Resources, Writing – review & editing. **Alexander Drzezga:** Conceptualization, Writing – review & editing. **Bernd Neumaier:** Conceptualization, Writing – review & editing.

Acknowledgments

This work was supported by the German Science Foundation (DFG) with the following grants: Heike Endepols: KFO 219 (EN439/4-1), EN439/6-1, Boris Zlatopolskiy: ZL65/1-1, ZL65/3-1.

Supplementary materials

Supplementary material associated with this article can be found, in the online version, at doi:10.1016/j.neuroimage.2021.118842.

References

Andrews, P.W., Bharwani, A., Lee, K.R., Fox, M., Thomson, J.A, 2015. Is serotonin an upper or a downer? The evolution of the serotonergic system and its role in depression and the antidepressant response. Neurosci. Biobehav. Rev. 51, 164–188.

Apetz, N., Kordys, E., Simon, M., Mang, B., Aswendt, M., Wiedermann, D., Neumaier, B., Drzezga, A., Timmermann, L., Endepols, H., 2019. Effects of subthalamic deep brain stimulation on striatal metabolic connectivity in a rat hemiparkinsonian model. Dis. Model. Mech. 12 (5), dmm039065.

Azmitia, E.C., 1981. Bilateral serotonergic projections to the dorsal hippocampus of the rat: simultaneous localization of 3H-5HT and HRP after retrograde transport. J. Comp. Neurol. 203, 737–743.

Badawy, A.A., 2017. Kynurenine pathway of tryptophan metabolism: regulatory and functional aspects. Int. J. Tryptophan Res. 10, 1178646917691938.

Barbosa, R., Scialfa, J.H., Terra, I.M., Cipolla-Neto, J., Simonneaux, V., Afeche, S.C., 2008. Tryptophan hydroxylase is modulated by L-type calcium channels in the rat pineal gland. Life Sci. 82, 529–535.

Berghauzen-Maciejewska, K., Wardas, J., Kosmowska, B., Domin, H., Smialowska, M., Glowacka, U., Ossowska, K., 2016. Adaptive down-regulation of the serotonin transporter in the 6-hydroxydopamine-induced rat model of preclinical stages of Parkinson's disease and after chronic pramipexole treatment. Neuroscience 314, 22–34.

Berumen, L.C., Rodriguez, A., Miledi, R., Garcia-Alcocer, G., 2012. Serotonin receptors in hippocampus. Sci. World J. 2012, 823493.

Best, J., Nijhout, H.F., Reed, M., 2010. Serotonin synthesis, release and reuptake in terminals: a mathematical model. Theor. Biol. Med. Model. 7, 34.

Campbell, B.M., Charych, E., Lee, A.W., Moller, T., 2014. Kynurenines in CNS disease: regulation by inflammatory cytokines. Front. Neurosci. 8, 12.

Chugani, D.C., Muzik, O., 2000. α [C-11] Methyl-L-tryptophan PET maps brain serotonin synthesis and kynurenine pathway metabolism. J. Cereb. Blood Flow Metab. 20, 2–9.

Cicchetti, F., Brownell, A.L., Williams, K., Chen, Y.I., Livni, E., Isacson, O., 2002. Neuroinflammation of the nigrostriatal pathway during progressive 6-OHDA dopamine degeneration in rats monitored by immunohistochemistry and PET imaging. Eur. J. Neurosci. 15, 991–998.

Dang, Y., Dale, W.E., Brown, O.R., 2000. Comparative effects of oxygen on indoleamine 2,3-dioxygenase and tryptophan 2,3-dioxygenase of the kynurenine pathway. Free Radic. Biol. Med. 28, 615–624.

De-Miguel, F.F., Leon-Pinzon, C., Noguez, P., Mendez, B., 2015. Serotonin release from the neuronal cell body and its long-lasting effects on the nervous system. Philos. Trans. R. Soc. Lond. B Biol. Sci. 370 (1672), 20140196.

Diksic, M., 2001. Labelled alpha-methyl-L-tryptophan as a tracer for the study of the brain serotonergic system. J. Psychiatry Neurosci. JPN 26, 293–303.

Eskow Jaunarajs, K.L., George, J.A., Bishop, C., 2012. L-DOPA-induced dysregulation of extrastriatal dopamine and serotonin and affective symptoms in a bilateral rat model of Parkinson's disease. Neuroscience 218, 243–256.

Gasparotto, J., Ribeiro, C.T., Bortolin, R.C., Somensi, N., Rabelo, T.K., Kunzler, A., Souza, N.C., Pasquali, M.A.B., Moreira, J.C.F., Gelain, D.P., 2017. Targeted inhibition of RAGE in substantia nigra of rats blocks 6-OHDA-induced dopaminergic denervation. Sci. Rep. 7, 8795.

Gutierrez, C.I., Urbina, M., Obregion, F., Glykys, J., Lima, L., 2003. Characterization of tryptophan high affinity transport system in pinealocytes of the rat. Day-night modulation. Amino Acids 25, 95–105.

Haas, S.J., Zhou, X., Machado, V., Wree, A., Krieglstein, K., Spittau, B., 2016. Expression of Tgfbeta1 and inflammatory markers in the 6-hydroxydopamine mouse model of Parkinson's disease. Front. Mol. Neurosci. 9, 7.

Jacobs, B.L., Azmitia, E.C., 1992. Structure and function of the brain serotonin system. Physiol. Rev. 72, 165–229.

Kageyama, T., Nakamura, M., Matsuo, A., Yamasaki, Y., Takakura, Y., Hashida, M., Kanai, Y., Naito, M., Tsuruo, T., Minato, N., Shimohama, S., 2000. The 4F2hc/LAT1 complex transports L-DOPA across the blood-brain barrier. Brain Res. 879, 115–121.

Kaminska, K., Lenda, T., Konieczny, J., Czarnecka, A., Lorenc-Koci, E., 2017. Depressive-like neurochemical and behavioral markers of Parkinson's disease after 6-OHDA administered unilaterally to the rat medial forebrain bundle. Pharmacol. Rep. 69, 985–994.

Knyihar-Csillik, E., Chadaide, Z., Mihaly, A., Krisztin-Peva, B., Fenyo, R., Vecsei, L., 2006. Effect of 6-hydroxydopamine treatment on kynurenine aminotransferase-I (KAT-I) immunoreactivity of neurons and glial cells in the rat substantia nigra. Acta Neuropathol. 112, 127–137.

Köhler, C., Steinbusch, H., 1982. Identification of serotonin and non-serotonin-containing neurons of the mid-brain raphe projecting to the entorhinal area and the hippocampal formation. A combined immunohistochemical and fluorescent retrograde tracing study in the rat brain. Neuroscience 7, 951–975.

Koprich, J.B., Reske-Nielsen, C., Mithal, P., Isacson, O., 2008. Neuroinflammation mediated by IL-1beta increases susceptibility of dopamine neurons to degeneration in an animal model of Parkinson's disease. J. Neuroinflamm. 5, 8.

Kordys, E., Apetz, N., Schneider, K., Duncan, E., Buschbell, B., Rohleder, C., Sue, M., Drzezga, A., Neumaier, B., Timmermann, L., Endepols, H., 2017. Motor impairment and compensation in a hemiparkinsonian rat model: correlation between dopamine depletion severity, cerebral metabolism and gait patterns. EJNMMI Res. 7, 68.

Lee, M., Ryu, Y.H., Cho, W.G., Jeon, T.J., Lyoo, C.H., Kang, Y.W., Lee, S.J., Kim, C.H., Kim, D.G., Kang, J.H., Seo, Y.B., Yi, C.H., Lee, K., Choi, T.H., Choi, J.Y., 2014. Dopaminergic neuron destruction reduces hippocampal serotonin 1A receptor uptake of trans-[18F]Mefway. Appl. Radiat. Isot. 94, 30–34.

Lee, M., Ryu, Y.H., Cho, W.G., Kang, Y.W., Lee, S.J., Jeon, T.J., Lyoo, C.H., Kim, C.H., Kim, D.G., Lee, K., Choi, T.H., Choi, J.Y., 2015. Relationship between dopamine deficit and the expression of depressive behavior resulted from alteration of serotonin system. Synapse 69, 453–460.

Lim, C.K., Fernandez-Gomez, F.J., Braidy, N., Estrada, C., Costa, C., Costa, S., Bessede, A., Fernandez-Villalba, E., Zinger, A., Herrero, M.T., Guillemin, G.J., 2017. Involvement of the kynurenine pathway in the pathogenesis of Parkinson's disease. Prog. Neurobiol. 155, 76–95.

Lin, L., Du, Y., Yuan, S., Shen, J., Lin, X., Zheng, Z., 2014. Serum melatonin is an alternative index of Parkinson's disease severity. Brain Res. 1547, 43–48.

Lin, L., Meng, T., Liu, T., Zheng, Z., 2013. Increased melatonin may play dual roles in the striata of a 6-hydroxydopamine model of Parkinson's disease. Life Sci. 92, 311–316.

Liu, K.C., Guo, Y., Zhang, J., Chen, L., Liu, Y.W., Lv, S.X., Xie, W., Wang, H.S., Zhang, Y.M., Zhang, L., 2019. Activation and blockade of dorsal hippocampal Serotonin6 receptors regulate anxiety-like behaviors in a unilateral 6-hydroxydopamine rat model of Parkinson's disease. Neurol. Res. 41, 791–801.

Mack, J.M., Schamne, M.G., Sampaio, T.B., Pertile, R.A., Fernandes, P.A., Markus, R.P., Prediger, R.D., 2016. Melatoninergic system in parkinson's disease: from neuroprotection to the management of motor and nonmotor symptoms. Oxidative Med. Cell. Longev. 2016, 3472032.

Maddison, D.C., Giorgini, F., 2015. The kynurenine pathway and neurodegenerative disease. Semin. Cell Dev. Biol. 40, 134–141.

Ng, K.Y., Leong, M.K., Liang, H., Paxinos, G., 2017. Melatonin receptors: distribution in mammalian brain and their respective putative functions. Brain Struct. Funct. 222, 2921–2939.

Olivier, B., 2015. Serotonin: a never-ending story. Eur. J. Pharmacol. 753, 2–18.

Pierucci, M., Di Matteo, V., Benigno, A., Crescimanno, G., Esposito, E., Di Giovanni, G., 2009. The unilateral nigral lesion induces dramatic bilateral modification on rat brain monoamine neurochemistry. Ann. N. Y. Acad. Sci. 1155, 316–323.

Politis, M., Loane, C., 2011. Serotonergic dysfunction in Parkinson's disease and its relevance to disability. Sci. World J. 11, 1726–1734.

Politis, M., Niccolini, F., 2015. Serotonin in Parkinson's disease. Behav. Brain Res. 277, 136–145.

Politis, M., Wu, K., Loane, C., Brooks, D.J., Kiferle, L., Turkheimer, F.E., Bain, P., Molloy, S., Piccini, P., 2014. Serotonergic mechanisms responsible for levodopa-induced dyskinesias in Parkinson's disease patients. J. Clin. Invest. 124, 1340–1349.

Qi, J., Leahy, R.M., Cherry, S.R., Chatziioannou, A., Farquhar, T.H., 1998. High-resolution 3D Bayesian image reconstruction using the microPET small-animal scanner. Phys. Med. Biol. 43, 1001–1013.

Richard, D.M., Dawes, M.A., Mathias, C.W., Acheson, A., Hill-Kapturczak, N., Dougherty, D.M., 2009. L-Tryptophan: basic metabolic functions, behavioral research and therapeutic indications. Int. J. Tryptophan Res. 2, 45–60.

Ruddick, J.P., Evans, A.K., Nutt, D.J., Lightman, S.L., Rook, G.A., Lowry, C.A., 2006. Tryptophan metabolism in the central nervous system: medical implications. Expert Rev. Mol. Med. 8, 1–27.

Schrag, A., Sauerbier, A., Chaudhuri, K.R., 2015. New clinical trials for nonmotor manifestations of Parkinson's disease. Mov. Disord. 30, 1490–1504.

Schroeder, D.C., Popp, E., Rohleder, C., Vus, S., Bethencourt, D.P., Finke, S.R., Zlatopolskiy, B.D., Zischler, J., Drzezga, A., Herff, H., Annecke, T., Hucho, T., Neumaier, B., Bottiger, B.W., Endepols, H., 2021. Positron emission tomography imaging of long-term expression of the 18kDa translocator protein after sudden cardiac arrest in rats. Shock 55, 620–629.

Schwarcz, R., Bruno, J.P., Muchowski, P.J., Wu, H.Q., 2012. Kynurenines in the mammalian brain: when physiology meets pathology. Nat. Rev. Neurosci. 13, 465.

Smith, S.M., Nichols, T.E., 2009. Threshold-free cluster enhancement: addressing problems of smoothing, threshold dependence and localisation in cluster inference. Neuroimage 44, 83–98.

Sodhi, R.K., Bansal, Y., Singh, R., Saroj, P., Bhandari, R., Kumar, B., Kuhad, A., 2021. IDO-1 inhibition protects against neuroinflammation, oxidative stress and mitochondrial dysfunction in 6-OHDA induced murine model of Parkinson's disease. Neurotoxicology 84, 184–197.

Swanson, L., 2003. Brain maps: Structure of the Rat Brain, 3rd ed. Academic Press, San Diego.

Szabo, N., Kincses, Z.T., Toldi, J., Vecsei, L., 2011. Altered tryptophan metabolism in Parkinson's disease: a possible novel therapeutic approach. J. Neurol. Sci. 310, 256–260.

Tan, L., Yu, J.T., Tan, L., 2012. The kynurenine pathway in neurodegenerative diseases: mechanistic and therapeutic considerations. J. Neurol. Sci. 323, 1–8.

Tordjman, S., Chokron, S., Delorme, R., Charrier, A., Bellissant, E., Jaafari, N., Fougerou, C., 2017. Melatonin: pharmacology, functions and therapeutic benefits. Curr. Neuropharmacol. 15, 434–443.

Tricoire, H., Locatelli, A., Chemineau, P., Malpaux, B., 2002. Melatonin enters the cerebrospinal fluid through the pineal recess. Endocrinology 143, 84–90.

Vertes, R.P., Fortin, W.J., Crane, A.M., 1999. Projections of the median raphe nucleus in the rat. J. Comp. Neurol. 407, 555–582.

Zadori, D., Klivenyi, P., Toldi, J., Fulop, F., Vecsei, L., 2012. Kynurenines in Parkinson's disease: therapeutic perspectives. J. Neural Transm. 119, 275–283 (Vienna).

Zarrad, F., Zlatopolskiy, B., Krapf, P., Zischler, J., Neumaier, B., 2017. A practical method for the preparation of ^{18}F-labeled aromatic amino acids from nucleophilic [^{18}F]fluoride and stannyl precursors for electrophilic radiohalogenation. Molecules 22, 2231.

Zlatopolskiy, B.D., Endepols, H., Krasikova, R.N., Fedorova, O.S., Ermert, J., Neumaier, B., 2020. 11C- and 18F-labelled tryptophans as PET-tracers for imaging of altered tryptophan metabolism in age-associated disorders. Russ. Chem. Rev. 89, 879–896.

Zlatopolskiy, B.D., Zischler, J., Krapf, P., Zarrad, F., Urusova, E.A., Kordys, E., Endepols, H., Neumaier, B., 2015. Copper-mediated aromatic radiofluorination revisited: efficient production of PET tracers on a preparative scale. Chem. Eur. J. 21, 5972–5979.

Zlatopolskiy, B.D., Zischler, J., Schäfer, D., Urusova, E.A., Guliyev, M., Bannykh, O., Endepols, H., Neumaier, B., 2018. Discovery of 7-[18F]fluorotryptophan as a novel positron emission tomography (PET) probe for the visualization of tryptophan metabolism in vivo. J. Med. Chem. 61, 189–206.